Capacitance-voltage profiling: Research-grade approach versus low-cost alternatives

Neal D. Reynolds, Cristian D. Panda, and John M. Essick[a)]
Physics Department, Reed College, Portland, Oregon 97202

(Received 21 July 2013; accepted 22 January 2014)

We describe an experiment that implements capacitance-voltage profiling on a reverse-biased Schottky barrier diode to determine the density of impurity dopants in its semiconductor layer as well as its built-in electric potential. Our sample is a commercially produced Schottky diode. Three different experimental setups, one using research-grade instrumentation, the other two using low-cost alternatives, are given and their results compared. In each of the low-cost setups, phase-sensitive detection required to measure the sample's capacitance is carried out using an inexpensive data acquisition (DAQ) device and a software program that implements a lock-in detection algorithm. The limitations of the DAQ device being used (e.g., restricted analog-to-digital conversion speed, inadequate waveform generation capabilities, lack of hardware triggering) are taken into account in each setup. Excellent agreement for the value of the doping density obtained by the all three setups is found and this value is shown to be consistent with the result of an independent method (secondary ion mass spectroscopy).
[http://dx.doi.org/10.1119/1.4864162]

I. INTRODUCTION

Semiconductor physics has proved itself a fertile field for advanced instructional laboratory developers. The properties of semiconductors engender natural student interest as they lie at the heart of modern-day technologies such as computers, smart phones, and the internet, while, pedagogically, semiconductor phenomena provide engaging applications of basic concepts in quantum mechanics, electrodynamics, and thermal physics. Hence, many semiconductor-related advanced laboratory experiments have been developed. For example, electrical measurements on forward-biased diodes and Hall devices have been used to measure the semiconducting band gap,[1–6] Schottky barrier height,[7] charge carrier density,[8–10] carrier transport properties,[11,12] and carrier statistical distributions.[13] Additionally, optical experiments are available to determine the band gap of bulk,[14,15] thin film,[16] and quantum-dot[17] semiconductor samples, the Maxwell-Boltzmann distribution of charge carriers,[18] and the vibration properties of nanomaterials.[19]

In this paper, we describe a newly developed instructional lab experiment that implements capacitance-voltage (CV) profiling on a reverse-biased Schottky barrier diode to determine the density of impurity dopants in its semiconductor layer, as well as its built-in electric potential. In contrast to the more complicated dual-semiconductor structure of a *pn*-junction diode, a Schottky barrier diode consists of a single semiconductor layer in contact with a metallic layer. Due to the simplicity of its construction, the functioning of a Schottky barrier diode can be explained theoretically using only introductory electrodynamics and semiconductor concepts. As with all semiconductor devices, fabrication of a high-quality Schottky diode requires specialized expertise and expensive deposition systems. To avoid this hurdle, we use a commercially produced Schottky barrier diode in this project. Additionally, in an effort to contain the cost of the capacitance characterization system, we describe several options for the setup, ranging from one consisting solely of stand-alone research-grade equipment to others that use low-cost op-amp circuitry and affordable computer-based instrumentation.

II. THEORY

A. Capacitance-voltage profiling of Schottky barrier

In this section, we derive the theoretical relations that are the basis of the capacitance-voltage profiling experimental technique.[20,22,23,25] First, consider a Schottky barrier of cross-sectional area A that consists of a metal layer in contact with an n-type semiconductor (dielectric constant ϵ; for silicon $\epsilon = 11.7$) and define an x-axis whose origin is at the metal-semiconductor interface with its positive direction toward the semiconductor's interior (Fig. 1). For the

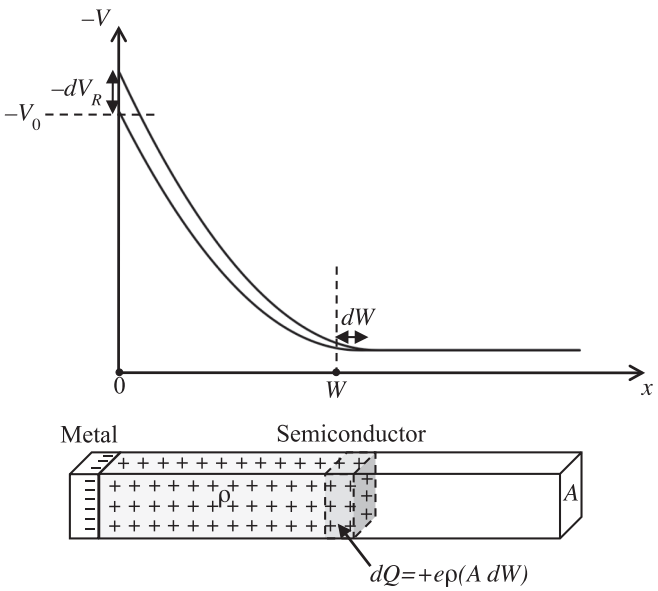

Fig. 1. Band bending in a Schottky barrier (cross-sectional area A) under bias of $-V_0$ creates a (shaded) depletion region of width W with space charge density $+e\rho$ due to ionized dopant atoms; ρ may be position-dependent. When the reverse bias is increased by dV_R, an additional charge of $dQ = +e\rho(AdW)$ is created at the tail of the depletion region. The metal-semiconductor interface is at $x = 0$ and it is assumed each ionized dopant atom has charge of $+e$.

semiconducting material, we assume the following. First, positively charged dopant atoms are incorporated in its lattice structure with a position-dependent volume number density ("doping density") $\rho(x)$. Second, its temperature is high enough so that these dopant atoms are fully ionized, that is, their extra electrons have all been promoted into the semiconductor's conduction band. These negative conduction electrons then perfectly compensate the dopant atom's positive charge so that, in its bulk, the semiconductor is electrically neutral. Third, at large x the semiconductor is connected to external circuitry via an ohmic "back contact."

We further assume that the type of metal is properly chosen so that when the two materials are joined, semiconductor conduction electrons transfer to the metal's surface, leaving behind a positively charged layer of uncompensated dopant atoms (called the "depletion region") in the volume of the semiconductor nearest the metal. This charge transfer takes place until the resulting space charge produces an electric potential $-V_{\text{bi}}$ at $x=0$ ($V_{\text{bi}} \geq 0$ is termed the "built-in potential"), which prevents further flow of charge (because the Fermi levels of the two materials have been equalized).

Then, if an externally applied voltage $-V_R$ (where $V_R \geq 0$ is called the "reverse bias") is applied at the metal contact so that the total potential at the metal-semiconductor interface is $-V_0 = -(V_R + V_{\text{bi}})$ and the total charge on the metal's surface is $-Q$, movement of semiconductor conduction electrons away from the interface (and out the back contact at large x) will extend the depletion region to a width W. Beyond the depletion region, the semiconductor is neutral and the effect of $-Q$ is not felt (i.e., the electric field is zero there). This effect is called dielectric screening and W is the "screening length."

Let's now analyze the special case of uniform doping density $\rho(x) = \rho_0$ (a constant), where each dopant atom is assumed to have a single charge $+e$. If the cross-sectional dimensions of the Schottky barrier are much greater than W, then by symmetry we can assume the electric field $\mathbf{E}$ in the depletion region points in the (negative) x-direction. Using the rectangular Gaussian surface shown in Fig. 2, with one of its end caps in the neutral bulk region (where $\mathbf{E}=0$) and the other end cap located a distance x from the metal-semiconductor interface, Gauss's law gives $\epsilon EA = +e\rho_0 A(W-x)/\epsilon_0$. For the electric potential $V(x)$ as a function of distance x into the depletion region, we have the two

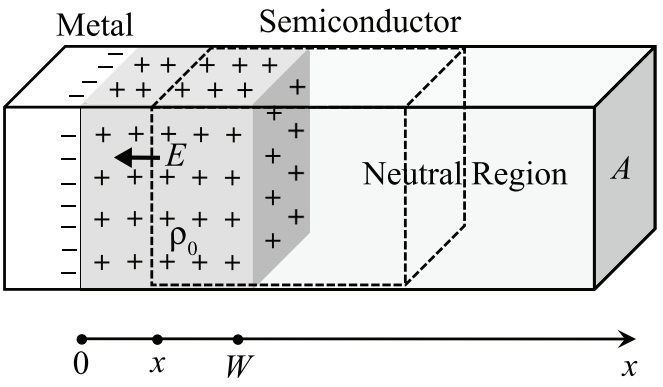

Fig. 2. Gauss's Law applied to a Schottky barrier (cross-sectional area A) under bias of $-V_0 = -(V_R + V_{\text{bi}})$ to determine the electric field E at location x, assuming constant doping density. By symmetry, the electric field E is directed along the (negative) x-axis. A (dashed) rectangular Gaussian surface is chosen with one face in the depletion region, where the space charge density is $+e\rho_0$; the other face is in neutral bulk region of the semiconductor, where the electric field is zero. The total charge within the Gaussian surface is $dQ = +e\rho_0 A(W-x)$.

boundary conditions: $V(0) = -(V_R + V_{\text{bi}})$ and $V(W) = 0$. Thus, from $V(W) - V(0) = -\int_0^W \mathbf{E}\cdot d\mathbf{x}$, we find

$$V_R + V_{\text{bi}} = \frac{e\rho_0}{2\epsilon\epsilon_0} W^2 \tag{1}$$

and so the width of the depletion region required to screen out the reverse bias V_R is

$$W = \sqrt{\frac{2\epsilon\epsilon_0 (V_R + V_{\text{bi}})}{e\rho_0}}. \tag{2}$$

If the reverse bias V_R is increased by a small amount dV_R, (remembering V_{bi} is a constant) we find from Eq. (1) that $dV_R = (e\rho_0/\epsilon\epsilon_0) W\, dW$, where dW is the increase in the depletion region's width. This increase in the depletion region width is due to flow of conduction electrons at the edge of the depletion region into the semiconductor's bulk (and out of the back contact), creating the extra space charge $dQ = +e\rho_0 (A\, dW)$ required to screen out the voltage change $-dV_R$ at the metal-semiconductor interface. By definition, this process produces a capacitive response given by

$$C \equiv \frac{dQ}{dV_R} = \frac{e\rho_0 (A dW)}{(e\rho_0/\epsilon\epsilon_0) W\, dW} = \frac{\epsilon\epsilon_0 A}{W}, \tag{3}$$

or, using Eq. (2), the Schottky barrier's capacitance as a function of reverse bias V_R is

$$C = A\sqrt{\frac{e\epsilon\epsilon_0\rho_0}{2(V_R + V_{\text{bi}})}}. \tag{4}$$

This expression can be re-written as

$$\frac{1}{C^2} = \frac{2}{A^2 e\epsilon\epsilon_0\rho_0}(V_R + V_{\text{bi}}), \tag{5}$$

suggesting the following capacitance-voltage characterization method: For a Schottky barrier with uniform doping density, a plot of $1/C^2$ versus V_R will yield a straight line with slope $m = 2/A^2 e\epsilon\epsilon_0\rho_0$ and y-intercept $b = 2V_{\text{bi}}/A^2 e\epsilon\epsilon_0\rho_0$. Then, the doping density and built-in potential are found from

$$\rho_0 = \frac{2}{A^2 e\epsilon\epsilon_0 m}, \tag{6}$$

and

$$V_{\text{bi}} = \frac{b}{m}. \tag{7}$$

The general case of position-dependent doping density $\rho(x)$ can be solved as follows: We start with the identity

$$\frac{d}{dx}\left(x\frac{dV}{dx}\right) = \frac{dV}{dx} + x\frac{d^2V}{dx^2}, \tag{8}$$

and note from Poisson's equation that

$$\frac{d^2V}{dx^2} = \frac{+e\rho(x)}{\epsilon\epsilon_0}. \tag{9}$$

Substituting Eq. (9) into Eq. (8) and integrating both sides of the resulting expression from $x=0$ to $x=W$ then yields

$$V_R + V_{\text{bi}} = \frac{e}{\epsilon\epsilon_0}\int_0^W x\rho(x)dx. \tag{10}$$

Now if the reverse bias V_R is increased by a small amount dV_R, the depletion region width will change by dW, creating the extra space charge $dQ = +e\rho(W)(A\,dW)$, where $\rho(W)$ is the doping density at the edge of the depletion region when the reverse bias is V_R. From Eq. (10), we have

$$d(V_R + V_{\text{bi}}) = \frac{e}{\epsilon\epsilon_0} d\left(\int_0^W x\rho(x)dx\right), \tag{11}$$

or

$$dV_R = \frac{e}{\epsilon\epsilon_0} W\rho(W)\,dW. \tag{12}$$

Thus, the capacitive response is given by

$$C \equiv \frac{dQ}{dV_R} = \frac{+e\,\rho(W)(A\,dW)}{(e/\epsilon\epsilon_0)W\,\rho(W)\,dW} = \frac{\epsilon\epsilon_0 A}{W}. \tag{13}$$

Re-writing this expression as $1/C^2 = (W/\epsilon\epsilon_0 A)^2$ and differentiating with respect to V_R gives

$$\frac{d}{dV_R}\left(\frac{1}{C^2}\right) = \frac{1}{(\epsilon\epsilon_0 A)^2} 2W \frac{dW}{dV_R}, \tag{14}$$

or, using Eq. (12),

$$\frac{d}{dV_R}\left(\frac{1}{C^2}\right) = \frac{1}{(\epsilon\epsilon_0 A)^2} 2W\left(\frac{\epsilon\epsilon_0}{eW\,\rho(W)}\right) = \frac{2}{A^2 e\epsilon\epsilon_0\,\rho(W)}. \tag{15}$$

Equation (15) is called the "Profiler's Equation" and can be used to characterize the spatial distribution of dopants in the semiconductor as follows: Starting with data for the Schottky barrier's capacitance C as a function of reverse bias V_R, a plot of $1/C^2$ versus V_R is constructed. At each value of reverse bias V_R on this plot, the slope $m = d(1/C^2)/dV_R$ is determined and the associated value of capacitance C noted. Then, each value of V_R corresponds to probing the doping density at the distance W from the metal-semiconductor interface, which is given by Eq. (13) to be

$$W = \frac{\epsilon\epsilon_0 A}{C}. \tag{16}$$

Using Eq. (15), the doping density at this distance W is determined by

$$\rho(W) = \frac{2}{A^2 e\epsilon\epsilon_0 m}. \tag{17}$$

To carry out capacitance-voltage characterization of a Schottky barrier diode, a negative dc voltage $-V_R$ is applied to its metal contact with the back contact grounded, producing a space-charge region of width W in the semiconductor. The barrier's capacitance C is then determined by adding a small ac modulation of amplitude V_{ac} and angular frequency ω to the applied voltage. To account for a small leakage current through the barrier and the resistance of the semiconductor's neutral bulk region, the Schottky diode is modeled as the parallel combination of the capacitor C and a leakage resistor R_L, in series with resistance R_S (see Fig. 3). In most cases, the semiconductor doping density is large enough so that R_S is negligible in comparison to the parallel combination of C and R_L. Taking $R_S \approx 0$, ac circuit analysis then predicts that the amplitude I of the total ac current flowing in this circuit is

$$I = \frac{V_{\text{ac}}}{Z} = V_{\text{ac}}\left(\frac{1}{R_L} + i\omega C\right) \equiv I_x + I_y. \tag{18}$$

Hence, relative to the applied ac voltage, the current will have an in-phase component I_x proportional to $1/R_L$ and a 90° out-of-phase ("quadrature") component I_y proportional to ωC. For a high-quality diode, the leakage current is small ($R_L \gg 1/\omega C$) so that $I_x \ll I_y$.

B. Lock-in detection algorithm

As we have seen, for the circuit described by Eq. (18), phase-sensitive detection of current is required to measure (a signal proportional to) capacitance. In our experimental setups, this phase-sensitive detection will be accomplished by using a lock-in amplifier,[26,27,32–35] which functions as follows: Assume that in response to an ac modulation input voltage $V_{\text{ac}}\sin(\omega_{\text{sig}}t)$, an experimental system produces an "in-phase" (relative to the input) output signal $V_{\text{sig}}\sin(\omega_{\text{sig}}t)$, where V_{sig} and ω_{sig} are the signal's amplitude and angular frequency, respectively. If we construct an "in-phase reference" sinusoid $2\sin(\omega_{\text{ref}}t)$ of amplitude 2 and angular frequency ω_{ref}, and take the product of the output signal and reference, we obtain

$$2V_{\text{sig}}\sin(\omega_{\text{sig}}t)\sin(\omega_{\text{ref}}t) = V_{\text{sig}}[\cos(\omega_{\text{sig}} - \omega_{\text{ref}})t - \cos(\omega_{\text{sig}} + \omega_{\text{ref}})t], \tag{19}$$

where we used the identity $\sin\alpha\sin\beta = 1/2[\cos(\alpha-\beta) - \cos(\alpha+\beta)]$. Thus, the multiplicative result is two ac sinusoids, each of amplitude V_{sig}, one with the "difference" frequency $(\omega_{\text{sig}} - \omega_{\text{ref}})$ and one with the "sum" frequency $(\omega_{\text{sig}} + \omega_{\text{ref}})$. Note that for the special case $\omega_{\text{ref}} = \omega_{\text{sig}}$, the difference-frequency sinusoid is the dc voltage V_{sig}. Hence, if the experiment's output waveform consists of a collection

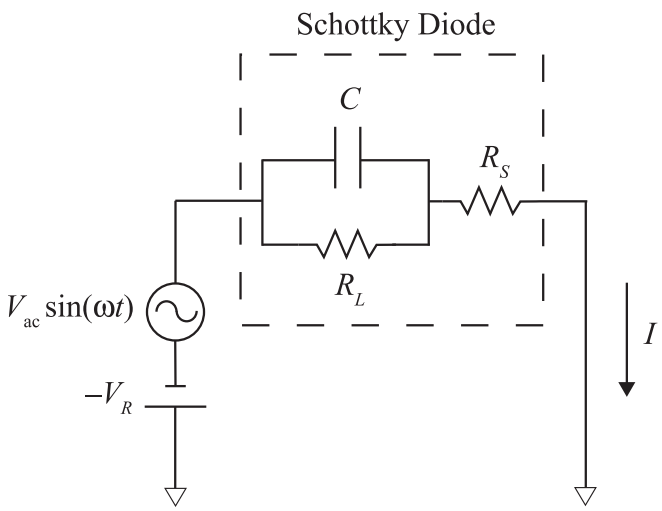

Fig. 3. Equivalent circuit of the CV characterization setup. The reverse-biased Schottky barrier diode is modeled as capacitance C in parallel with leakage resistance R_L. The semiconductor's neutral bulk region (beyond the depletion region) contributes a series resistance R_S. For a high-quality diode, the impedance of R_L is much greater than that of C and R_S is negligible. Thus, the response of the diode to the small ac modulation voltage is predominately due to C.

of component sinusoids of various frequencies, by multiplying this waveform by $2\sin(\omega_{\text{ref}}t)$ and then using low-pass filtering to find only the resultant dc value, one can determine the amplitude of the "in-phase" sinusoidal component within the output waveform whose frequency equals that of the reference.

In a similar way, if the experimental system produces a "quadrature" output signal $V_{\text{sig}}\cos(\omega_{\text{sig}}t)$ in response to the input voltage $V_{\text{ac}}\sin(\omega_{\text{sig}}t)$, by multiplying this output signal by the "quadrature reference" $2\cos(\omega_{\text{ref}}t)$ and low-pass filtering for the resultant dc value, this dc value will equal V_{sig} (i.e., the quadrature signal amplitude).

III. EXPERIMENTAL SETUPS AND RESULTS

Our goal is to demonstrate both research-grade and low-cost (but accurate) implementations of the capacitance profiling technique for use in instructional laboratories. We first carry out the capacitance-voltage (CV) method using research-grade, stand-alone instrumentation in order to show how the technique works, and also to establish a baseline of precision by which to judge the accuracy of our lower-cost setups. Next, we show two inexpensive computer-based versions of this experiment, each based on an affordable USB-interfaced data acquisition device, which produce excellent results.

For each variant of the experiment, our sample is a commercially produced Schottky diode. Because the measured signal is proportional to the capacitor's cross-sectional area A, we chose a Schottky diode with a large-area metallic contact [Semiconix Semiconductor STPS20120D (Ref. 28)]. The contact is composed of a TiW alloy. We stripped the epoxy encapsulation from one of these devices[29] to expose the diode and used a calibrated microscope to measure the square contact[30] to have a side length of (2.32 ± 0.02) mm, yielding $A = 5.38 \pm 0.09$ mm^2. On this exposed diode, secondary ion mass spectroscopy (SIMS)[31] established that its n-type silicon layer has a phosphorous doping density of approximately 3×10^{15} dopants/cm^3, while no arsenic (another common n-type dopant atom in silicon) was detected.

At zero applied bias, the capacitance of the STPS20120D diode is on the order of 1000 pF. For all of the experiments described in this paper, the ac modulation amplitude and frequency are $V_{\text{ac}} = 30$ mV rms and $f = 1000$ Hz, respectively, and the reverse bias V_R is scanned over the range from 0.0–9.9 V in increments of 0.1 V. To allow for settling of the measured signal, a wait of 10 lock-in time constants is taken before reading each data point during the scan. The modulation amplitude is chosen to be less than the reverse-bias increment so that each value of V_R in our scan probes a unique position in our sample; the choice of frequency is dictated by the maximum sampling rate of the USB-6009 DAQ device (see discussion below).

A. Research-grade implementation

A schematic diagram of our research-grade experimental setup is shown in Fig. 4. A USB-interfaced Agilent 33210 A function generator applies the ac oscillation of small amplitude V_{ac} and frequency f along with a dc offset $-V_R$ to the Schottky diode's metal contact. The other end of the diode is connected to a DL Instruments 1211 current preamplifier, which is a virtual electrical ground and converts the diode's current I to a voltage $V = \beta I$, where the proportionality constant $\beta = 10^6$ V/A. For the diode and data-taking parameters

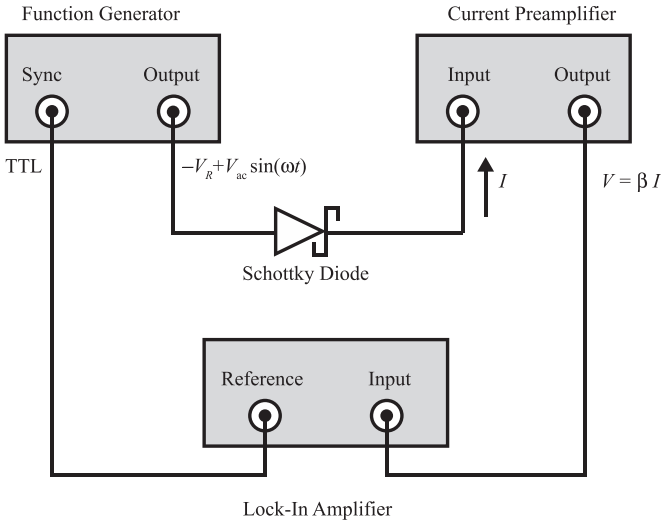

Fig. 4. Research-grade implementation of capacitance profiling method using stand-alone instrumentation (Agilent 33210 A function generator, DL Instruments 1211 current preamplifier, Stanford Research System SR830 lock-in amplifier).

we use, the resulting value for V is on the order of $\beta \times (V_{\text{ac}}\,\omega C) = 10^6\ \text{V/A} \times [(30\,\text{mV rms})2\pi(1000\,\text{Hz})(10^{-9}\,\text{F})] \approx 200\,\text{mV rms}$. This voltage is then read by a GPIB-interfaced Stanford Research System SR830 lock-in amplifier. The function generator's TTL sync output is used as the lock-in's reference signal, with zero phase defined by the moment of the negative-going zero crossing of the ac oscillation (that is, the moment at which the reverse bias begins to increase). Since, at constant frequency, the lock-in measures a quadrature voltage that is proportional (via β) to the circuit's quadrature current, which in turn is proportional to C [see Eq. (18)], a calibration capacitor[36] of known capacitance C_0 is substituted in the circuit for the Schottky diode and the resultant quadrature voltage output V_{0y} is measured. Then, with the diode replaced back into the circuit, its capacitance C in response to a particular reverse bias is determined by measuring the quadrature voltage V_y and using the proportionality relation: $C/C_0 = V_y/V_{0y}$. Data taking is controlled by a LabVIEW program.

To account for small (on the order of a few degrees in most cases) phase shifts due to other sources (e.g., cabling, amplifiers) than the capacitances of interest, a further refinement called "autophasing" can be included as follows: With the calibration capacitor replacing the Schottky diode in the circuit, record V_{x0} and V_{y0}, which are the lock-in's in-phase and quadrature readings for the known calibration capacitor C_0, respectively. Then, assuming the calibration capacitor has a purely capacitive impedance (that is, it has zero leakage current), these two readings determine a vector in the complex impedance plane that defines the direction of the sample's capacitive response. With the diode back in the circuit, its in-phase and quadrature voltages V_x and V_y are measured. These two readings determine a vector describing the sample's ac response in the complex impedance plane. By mathematically finding the component of the sample's response along the purely capacitive direction (via a dot product), the relation for the sample's capacitance is obtained as

$$C = \frac{(V_x V_{x0} + V_y V_{y0})}{V_{x0}^2 + V_{y0}^2} C_0. \tag{20}$$

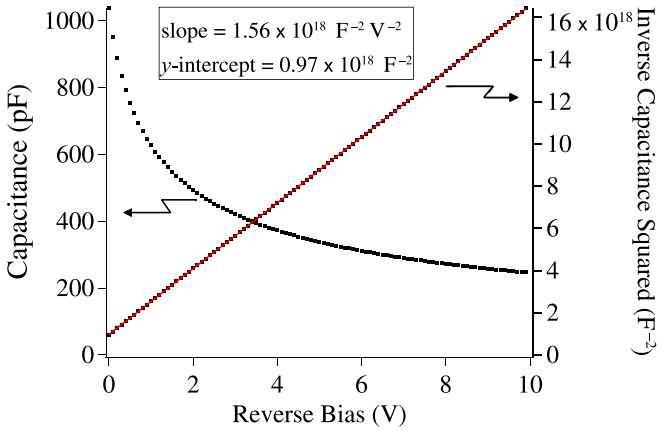

Fig. 5. Experimental data (C vs V_R and $1/C^2$ vs V_R) taken at room temperature on a STPS20120D Schottky diode using research-grade instrumentation (time constant of lock-in is $\tau = 300$ ms). The latter plot determines the diode's constant doping density and built-in potential to be 2.7×10^{15} dopants/cm^3 and 0.622 V, respectively. Error bar for each data point is smaller than symbol used to represent point.

Commercial research-grade lock-in amplifiers commonly offer autophasing with the push of a button. For software-based lock-ins, autophasing can be accomplished by including Eq. (20) in the software program.

The room-temperature capacitance versus reverse bias data acquired on a STPS20120D diode, along with the resulting $1/C^2$ vs V_R plot, are shown in Fig. 5. The straight-line character of the latter plot indicates that the diode's doping density is constant over the spatial region profiled. Using Eqs. (6) and (7), the slope and y-intercept of this plot determine that the doping density in this region and the diode's built-in potential are 2.7×10^{15} dopant/cm^3 and 0.622 V, respectively (in semiconductor physics, it is typical to give doping density in units of dopant/cm^3, rather than dopant/m^3). Our value for V_{bi} agrees with published values obtained on titanium-tungsten silicide Schottky contacts.[37]

The uncertainties in our ρ and V_{bi} values obtained from Eqs. (6) and (7) were estimated as follows. First, the influence of random measurement error in introducing uncertainty in our straight-line fit of the $1/C^2$ versus V_R plot was gauged by comparing the results of ten identical runs of the experiment. We found that such random errors contributed uncertainty in m and b on the order of only 0.1%. Thus, in using Eq. (6), the uncertainty in the contact area is the dominant contribution to $\delta\rho$. With $\delta A/A \approx 0.02$, we get $\delta\rho = 0.1 \times 10^{15}$ dopant/cm^3. To determine V_{bi} via Eq. (7), only the highly accurate m and b values are involved. With $\delta m/m \approx \delta b/b \approx 0.001$, our model predicts $\delta V_{bi} \approx 0.001$ V. However, one might question whether our model for the Schottky barrier, which ignores secondary effects such as series resistance and small temperature corrections, describes a real-life diode to this level of accuracy (literature values for V_{bi} obtained from CV measurements are typically given with only two digits of precision).[20,24]

Using these same CV data, Eqs. (16) and (17) yield the $\rho(W)$ versus W plot shown in Fig. 6. Also shown in this plot are the SIMS data for phosphorous dopant density versus distance from the metal-semiconductor interface taken on this sample. The SIMS detection limit for phosphorous is 1×10^{15} dopant/cm^3, so the SIMS data taken on our sample are somewhat noisy. Averaged over the spatial region from $W = 0.5$ to 1.0 μm, the SIMS doping density is $(3 \pm 2) \times 10^{15}$ dopant/cm^3. Thus, the doping densities determined by the capacitance and SIMS characterization techniques are consistent.

Finally, we observe in Fig. 6 that the capacitance profiling value for $\rho(x)$ becomes more noisy as W increases. This well-known effect[21,38] is explained as follows. From Eq. (17), the uncertainty $\delta\rho$ in the doping density determined at each location $x = W$ is given by $\delta\rho/\rho = \delta m/m$, where δm is the uncertainty in determining the slope $m = d(1/C^2)/dV_R$ at that location (for this calculation, the same value for A is used at all locations, so the uncertainty in contact area does not contribute to the observed scatter of ρ-values). Writing m in terms of our measured quantities, we see that the slope at

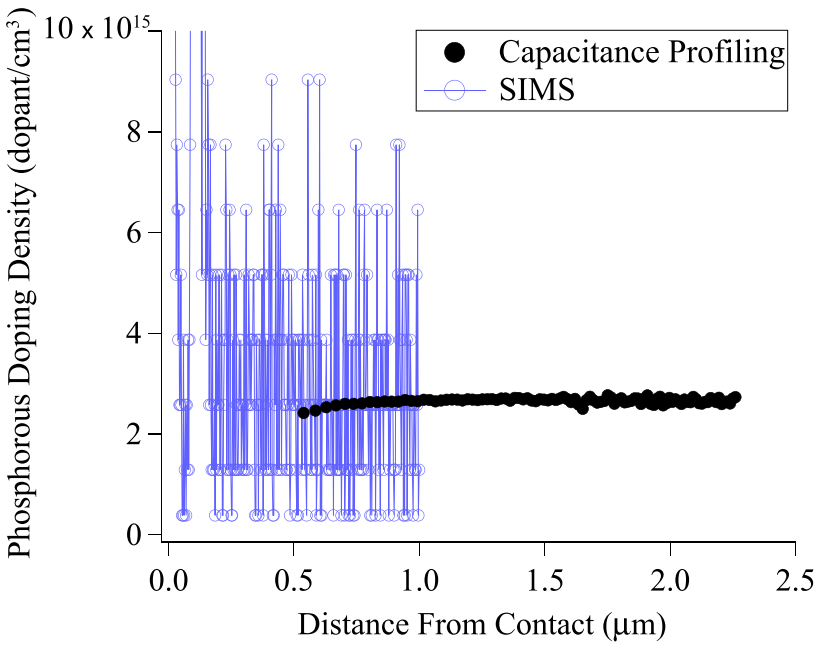

Fig. 6. Spatial profile of phosphorous doping. The capacitance profiling result (solid circles) is found using Eqs. (16) and (17), where the x-axis is plotting W. The minimum value of W is determined by V_{bi}. The SIMS result (open circles) gives an average of 3×10^{15} dopant/cm^3 in the region that overlaps with that profiled by the capacitance method.

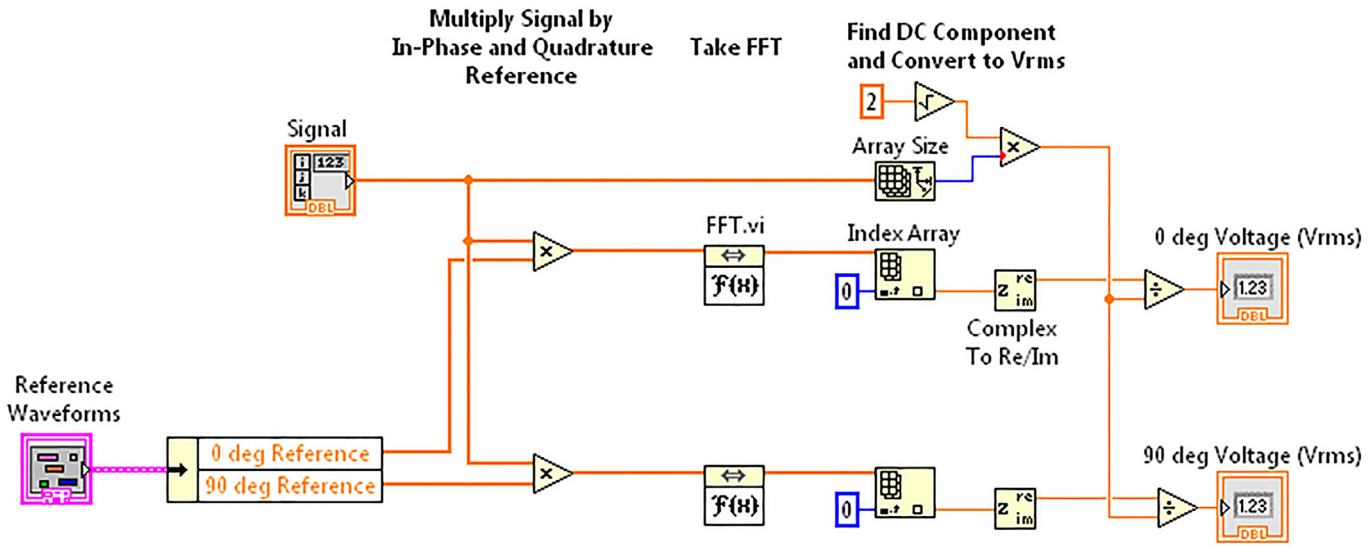

Fig. 7. LabVIEW code to carry out two-phase lock-in amplifier algorithm. A fast Fourier Transform performs the required low-pass filtering to obtain the dc value, which is the zero-index element in the array output by the FFT.vi icon.

$x = W$ is calculated by $m \approx (-2/C^3)\Delta C/\Delta V_R$, where ΔC and ΔV_R are the differences between neighboring values of capacitance and reverse bias at that location, respectively. In our data scans, $\Delta V_R = 0.100\,\mathrm{V}$ at all locations and so the uncertainty in this quantity cannot explain the increase in $\delta\rho$ at increasing W. Conversely, as shown in Fig. 5, the CV curve flattens out at larger biases and thus the difference ΔC in neighboring capacitance values is smaller and more susceptible to random measurement error as V_R (and its associated W) increases. Keeping just this relevant contribution to uncertainty, we get $\delta m/m \approx \delta(\Delta C)/\Delta C$. Since ΔC is the difference between two neighboring capacitance values, each with an uncertainty of δC, we find $\delta(\Delta C) = \sqrt{2}\delta C$. Also, from Eq. (13), we have $\Delta C \approx (-\epsilon\epsilon_0 A/W^2)\Delta W$. Putting Eq. (12) into this expression, we find $\Delta C \approx (-\epsilon^2\epsilon_0^2 A/e\rho W^3)\Delta V_R$, and thus

$$\frac{\delta\rho}{\rho} = \frac{\delta m}{m} \approx \frac{\delta(\Delta C)}{\Delta C} \approx \frac{\sqrt{2}\,\delta C}{(-\epsilon^2\epsilon_0^2 A/e\rho W^3)\Delta V_R} \approx -\left(\frac{\sqrt{2}e}{\epsilon^2\epsilon_0^2 A}\right)\left(\frac{\rho\delta C}{\Delta V_R}\right)W^3. \tag{21}$$

In our scans, δC and ΔV_R are constant and ρ is found to be uniform in our sample. Thus, Eq. (21) predicts that $\delta\rho$ will be proportional W^3, explaining why the doping density becomes markedly more noisy as we profile deeper into the sample (alternate profiling methods have been developed that use constant electric field increments, rather than constant reverse bias steps, which somewhat alleviate this noise problem at larger profiling depths). From the data in Fig. 6 we determine that in the range $W = 2.00$–$2.25\,\mu\mathrm{m}$, $\delta\rho = 4.4 \times 10^{13}$ dopant/cm^3. Using this value, along with the other known quantities in Eq. (21), we find that $\delta C = 0.02\,\mathrm{pF}$ is responsible for the observed scatter in ρ.

B. Low-cost implementation

We now demonstrate that similar results can be obtained from two different low-cost experimental setups. In each of these setups, the commercial current preamplifier is replaced by a simple current-to-voltage (I-to-V) op-amp circuit with a $10^6\ \Omega$ feedback resistor so that $\beta = -10^6\,\mathrm{V/A}$. In addition, the required phase-sensitive detection is carried out using a computer-based lock-in amplifier[40–42] consisting of an inexpensive data acquisition (DAQ) device and a LabVIEW software program. The central features of this computer-based lock-in are as follows: First, triggered by the negative-going transition of a function generator's TTL (or square-wave) sync output, the DAQ device acquires N (a power of two) samples of the I-to- V circuit's voltage output. The sampling rate is chosen to be $f_{\mathrm{sampling}} = N_{\mathrm{point}} \times f$, where N_{point} is the number of samples to acquire during one reference cycle and f is the reference frequency. A total of N_{cycle} reference cycles are acquired so that the total number of acquired voltage samples is $N = N_{\mathrm{point}} \times N_{\mathrm{cycle}}$. Since the digitizing process is triggered at the our defined zero-phase angle, in software we create two copies of this acquired data waveform and multiply one copy by the "in-phase" reference $2\sin(2\pi ft)$ and the other copy by the "quadrature" reference $2\cos(2\pi ft)$. A fast Fourier transform is then taken of each of these arrays (hence the reason N is chosen to be a power of two) and the dc components of each picked out, resulting in the in-phase and quadrature voltage amplitude at frequency f in the original digitized waveform. Thus, the frequency bandwidth of our output signal is on the order of the FFT's frequency resolution[39] $\Delta f = f_{\mathrm{sampling}}/N$. We define the time constant of our lock-in algorithm to be $\tau \equiv 1/\Delta f$, so $\tau = N/f_{\mathrm{sampling}} = (N_{\mathrm{point}}N_{\mathrm{cycle}})/(N_{\mathrm{point}}f) = N_{\mathrm{cycle}}/f$. Figure 7 illustrates how this lock-in algorithm is programmed in LabVIEW.[43]

We will describe how to carry out the above-described scheme with two different commonly used low-cost DAQ devices: the USB-6009 and the myDAQ.[44] In each case, the manner in which the scheme is implemented must be adapted to the limitations of the DAQ device.

1. Setup using the USB-6009

The USB-6009 device performs 14-bit analog-to-digital conversions of an incoming signal at rates up to 48,000 Samples per second (S/s). Each N-sample acquisition can be

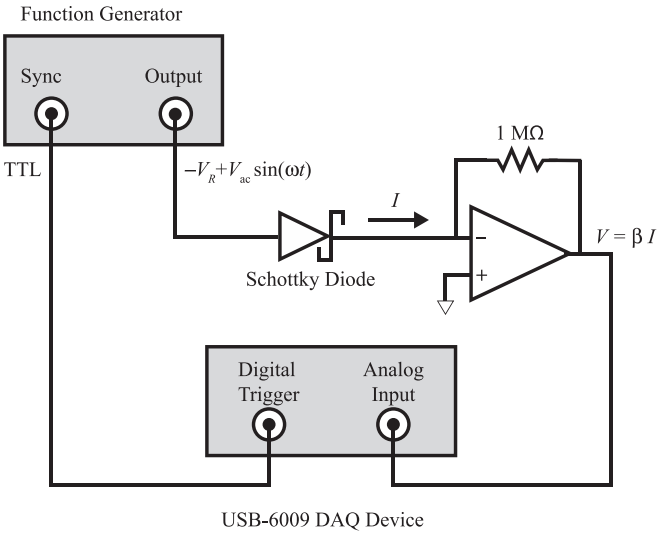

Fig. 8. Low-cost implementation of capacitance profiling using USB-60009 DAQ device. The op-amp (LF411) circuit serves as a current preamplifier and the lock-in algorithm is carried out using a hardware-triggered DAQ device and LabVIEW software. Because the DAQ device has minimal waveform generation capabilities, a stand-alone computer-interfaced Agilent 33210 A function generator is used.

hardware triggered by a TTL signal. The device's programmable-gain amplifier allows for eight possible input voltage ranges over which to spread the 14-bit resolution. Since our input signal is on the order of a few hundred millivolts, we choose the (device's most sensitive) ± 1 V range. Additionally, given the 48 kS/s maximum sampling rate and that fact that we need the number of samples per cycle (N_{point}) to be a power of two, we chose our reference frequency to be 1000 Hz. Then, N_{point} can be 32, the minimum value we feel necessary to properly describe the 1000-Hz signal. Finally, this DAQ device possesses only modest digital-to-analog conversion capabilities. With a maximum analog output update rate of 150 Hz, the USB-6009 cannot produce the reference signal we require for our experiment. Hence, we retain the USB-interfaced Agilent 33210 A function generator for this setup, as shown in Fig. 8.

With $f = 1000$ Hz, we chose $N_{\text{point}} = 32$ and $N_{\text{cycle}} = 512$. Then, $f_{\text{sampling}} = 32{,}000$ S/s, $N = 16{,}384$ ($=2^{14}$), and $\tau = 0.51$ s. Using these parameters, the room-temperature capacitance versus reverse bias data was acquired on a STPS20120D diode. The resulting $1/C^2$ vs V_R plot is shown in Fig. 9. The straight-line character of this plot indicates that the diode's doping density is constant over the spatial region profiled. Using Eqs. (6) and (7), the slope and y-intercept of this plot determine that the doping density in this region and the diode's built-in potential are 2.6×10^{15} dopant/cm^3 and 0.613 V, respectively. These results are in excellent agreement with the results obtained using research-grade instrumentation.

As with the research-grade setup, the uncertainties in our ρ and V_{bi} values were estimated by first comparing the results of ten identical runs of the experiment. We found that such random errors contributed uncertainties in m and b on the order of only 0.5%. So, again, the uncertainty in the contact area is the dominant contribution to $\delta\rho$, yielding $\delta\rho = 0.1 \times 10^{15}$ dopant/cm^3. With $\delta m/m \approx \delta b/b \approx 0.005$, we predict $\delta V_{\text{bi}} \approx 0.004$ V.

Using these same CV data, Eqs. (16) and (17) yield the $\rho(W)$ vs W plot shown in Fig. 10. This plot indicates constant doping

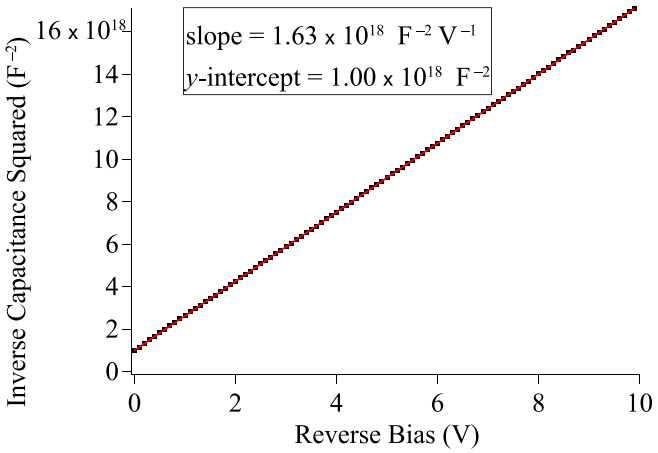

Fig. 9. Experimental data ($1/C^2$ vs V_R) obtained at room temperature on a STPS20120D Schottky diode using USB-6009 DAQ device (time constant of lock-in is $\tau = 510$ ms). This plot determines the diode's constant doping density and built-in potential to be 2.6×10^{15} dopant/cm^3 and 0.613 V. Error bar for each data point is smaller than symbol used to represent point.

density over the region profiled and again is in excellent agreement with the research-grade results (Fig. 6). We note that, as described by Eq. (21), the doping density determination becomes more noisy as the profile probes deeper into the sample. This noise is more noticeable in Fig. 10 than in Fig. 6 because δC is larger for the USB-6009 setup. From the data in Fig. 10, we determine that in the range $W = 2.00$–2.25 μm, $\delta\rho = 1.6 \times 10^{14}$ dopant/cm^3. Using this value, along with the other known quantities in Eq. (21), we find that $\delta C = 0.07$ pF is responsible for the observed scatter in ρ.

2. *Setup using the myDAQ*

The myDAQ device performs 16-bit analog-to-digital conversions of an incoming signal at rates up to 200,000 S/s. The device's programmable-gain amplifier allows for two possible input voltage ranges. We choose the (device's most sensitive) ± 2 V range. However, the device offers no hardware triggering capability for these digitizing operations. Thus, the triggering for the voltage acquisitions must be done in software. Finally, this DAQ device can also perform

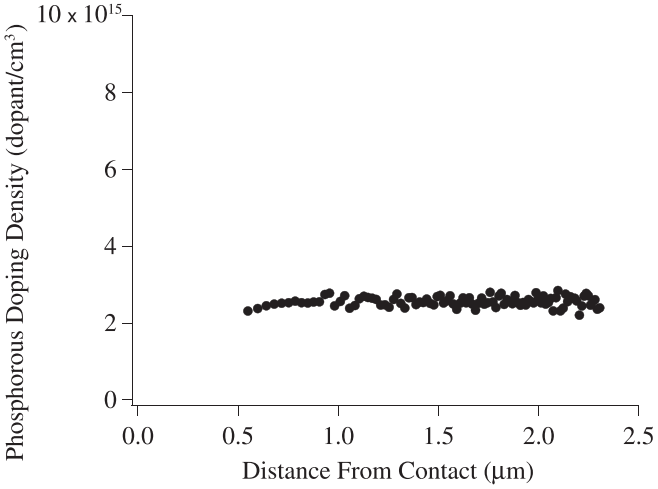

Fig. 10. Spatial profile of phosphorous doping obtained using a USB-6009 DAQ device. A constant value for $\rho(x)$ of about 2.6×10^{15} dopant/cm^3 is indicated over the spatial range $W = 0.5$–2.3 μm.

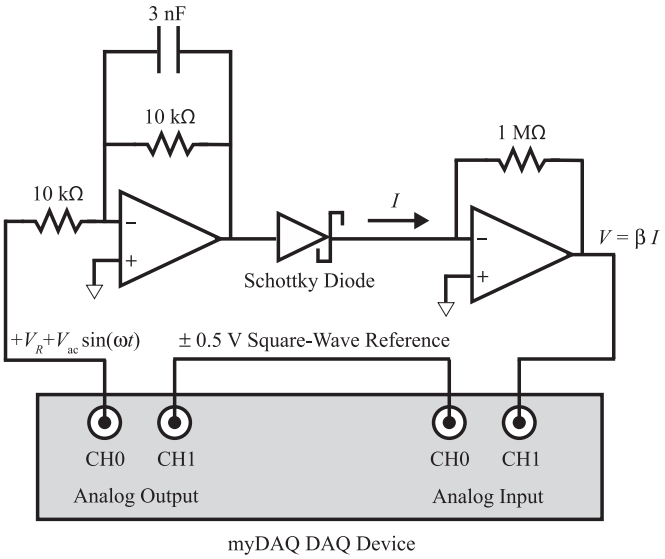

Fig. 11. Low-cost implementation of capacitance profiling using a myDAQ DAQ device. The op-amp (LF411) circuit serves as a current preamplifier and the lock-in algorithm is carried out using a software-triggered DAQ device and LabVIEW software. The waveform generation function of the myDAQ device is used to create a modulated reverse bias. The op-amp low-pass filter with $f_{3dB} \approx 5$ kHz suppresses digitizing steps on small-amplitude ac modulation.

digital-to-analog conversions at rates up to 200,000 S/s on two analog output (AO) channels. We use these two AO channels, each operating at 200 kS/s, to produce our required modulated bias voltage as well as a digital reference signal, whose transitions are in-phase with the bias voltage's ac modulation. As shown in Fig. 11, a ± 0.5 V square-wave reference signal generated by one of the analog output channels is directly connected to, and read by, one of the analog input channels. The moment at which a transition of this square wave occurs is determined by searching the acquired waveform in software, enabling lock-in detection. Also, the modulated bias voltage produced by the other AO channel is passed through an (inverting) op-amp low-pass filter in order

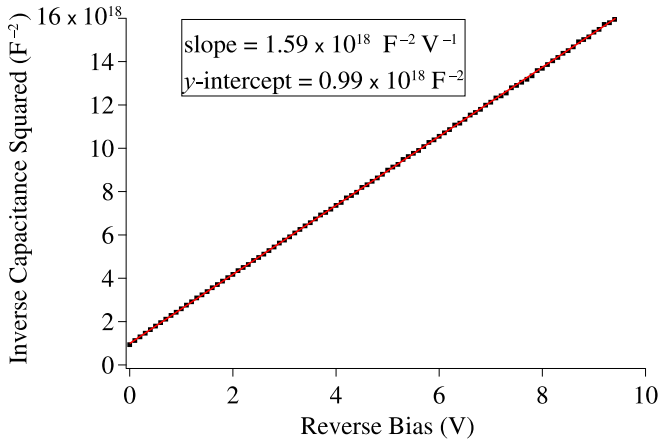

Fig. 13. Experimental data ($1/C^2$ vs V_R) obtained at room temperature on a STPS20120D Schottky diode using a myDAQ DAQ device (time constant of lock-in is $\tau = 130$ ms). This plot determines the diode's constant doping density and built-in potential to be 2.6×10^{15} dopant/cm^3 and 0.623 V. Error bar for each data point is smaller than symbol used to represent point.

to suppress digital quantization. Figure 12 illustrates how software triggering is carried out in LabVIEW.

With $f = 1000$ Hz, we chose $N_{point} = N_{cycle} = 128$. Then, $f_{sampling} = 128{,}000$ S/s, $N = 16{,}384$ $(=2^{14})$, and $\tau = 0.13$ s. Using these parameters, the room-temperature capacitance versus reverse bias data was acquired on a STPS20120D diode. The resulting $1/C^2$ vs V_R plot is shown in Fig. 13. Again, the straight-line character of this plot indicates that the diode's doping density is constant over the spatial region profiled. Using Eqs. (6) and (7), the slope and y-intercept of this plot determine that the doping density in this region and the diode's built-in potential are 2.6×10^{15} dopants/cm^3 and 0.623 V, respectively. These results are in excellent agreement with those obtained using the other setups.

As before, the uncertainties in our ρ and V_{bi} values were estimated by first comparing the results of ten identical runs of the experiment. We found that such random errors contributed uncertainties in m and b on the order of 0.6%. Thus,

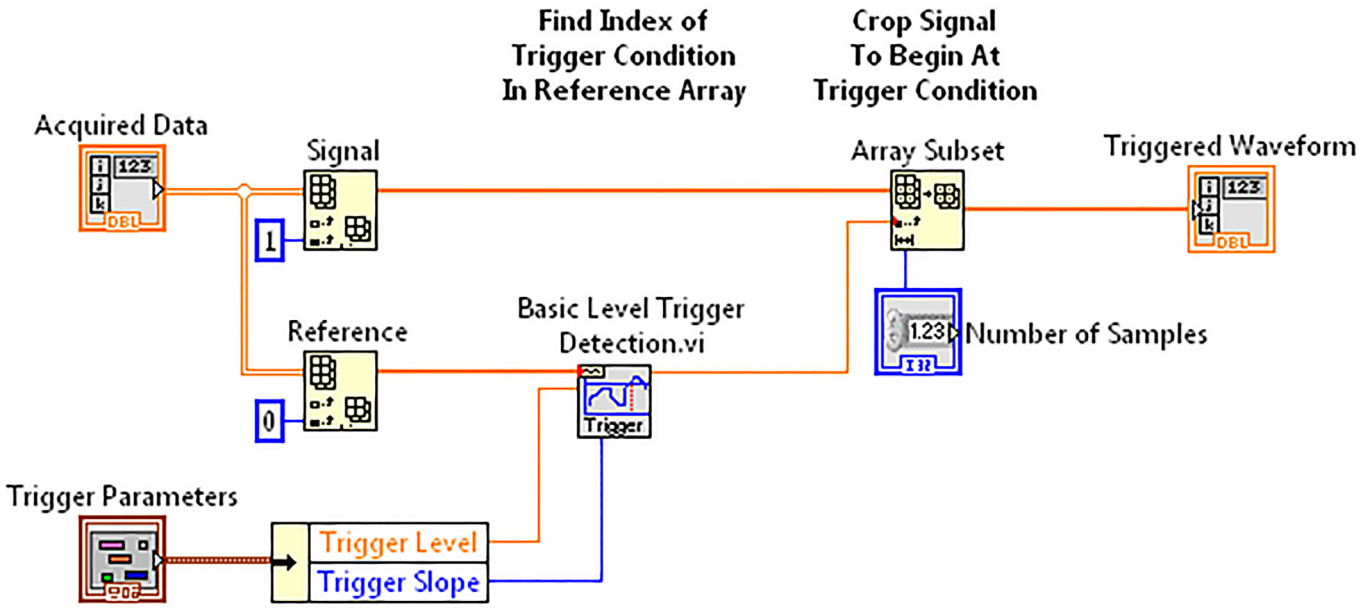

Fig. 12. LabVIEW code to carry out software analog triggering.

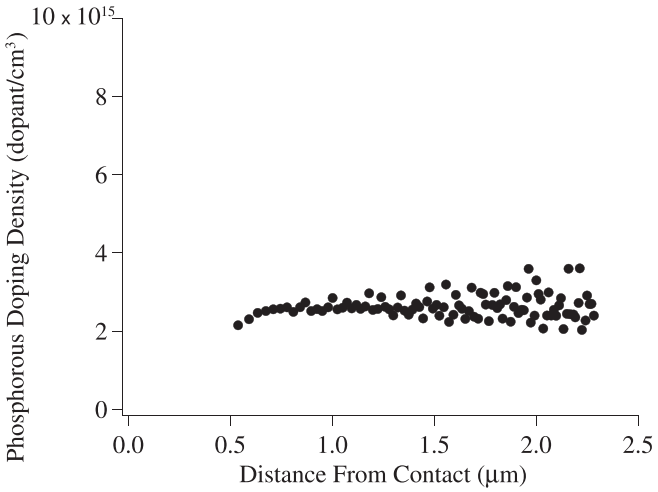

Fig. 14. Spatial profile of phosphorous doping obtained using the myDAQ DAQ device. The noise in smaller capacitance values (at greater depletion-region widths) causes the evaluation of the derivative in the Profiler's Equation to be inaccurate at $W > 1.5\,\mu$m.

δA is the dominant contribution to $\delta\rho$, yielding $\delta\rho = 0.1 \times 10^{15}$ dopant/cm^3. With $\delta m/m \approx \delta b/b \approx 0.006$, we predict $\delta V_{\text{bi}} \approx 0.005$ V.

Using these same CV data, Eqs. (16) and (17) yield the $\rho(W)$ vs W plot shown in Fig. 14. Again, we see that, per Eq. (21), the doping density determination becomes more noisy as the profile probes deeper into the sample. This time the noise is significantly larger than in Figs. 6 and 10, indicating that δC is larger for the myDAQ setup in comparison to the two other setups used. From the data in Fig. 14, we determine that in the range $W = 2.00$–$2.25\,\mu$m, $\delta\rho = 4.4 \times 10^{14}$ dopant/cm^3. Using this value, along with the other known quantities in Eq. (21), we find that $\delta C = 0.2$ pF is responsible for the observed scatter in ρ. This larger uncertainty in the capacitance measurement (in comparison to the other two setups) most likely derives from the lower-level of precision inherent in the software triggering used here.

IV. CONCLUSION

A summary of our results is given in Table I. Here, we see excellent agreement between the three setups, with possibly slight systemic shifts due to the different lock-in detection scheme, cabling, and breadboard wiring used in each case.

In conclusion, using research-grade instrumentation, we have demonstrated the capacitance profiling method and verified its results are consistent with another characterization technique (secondary ion mass spectroscopy). Further, we have shown that, in spite of their limitations such as restricted analog-to-digital conversion speed, inadequate waveform generation capabilities, and lack of hardware triggering, inexpensive DAQ devices can be used to accurately carry out capacitance profiling on semiconductor samples. These low-cost solutions make the introduction of such measurements an attractive option for advanced laboratory projects.

Table I. Summary of results on STPS20120D Schottky diode.

Setup	ρ ($\times 10^{15}$ dopants/cm^3)	V_{bi} (V)	δC (pF)
Research-grade	2.7 ± 0.1	0.622 ± 0.001	0.02
USB-6009[a]	2.6 ± 0.1	0.613 ± 0.004	0.07
myDAQ[b]	2.6 ± 0.1	0.623 ± 0.005	0.2
SIMS[c]	3 ± 2	–	–

[a]Hardware triggering, audio-range 14-bit data acquisition, inadequate waveform generation.
[b]Software triggering only, excellent 16-bit data acquisition and waveform generation rates.
[c]Performed by Evans analytical group.

ACKNOWLEDGMENTS

This work is dedicated to the memory of Professor J. David Cohen.

[a]Electronic mail: jessick@reed.edu

[1]J. W. Precker and M. A. da Silva, "Experimental estimation of the band gap in silicon and germanium from the temperature-voltage curve of diode," Am. J. Phys. **70**, 1150–1153 (2002).
[2]H. Jaeger, M. J. Pechan, and D. K. Lottis, "Materials physics: A new contemporary undergraduate laboratory," Am. J. Phys. **66**, 724–730 (1998).
[3]A. Sconza, G. Torzo, and G. Viola, "Experiment on the physics of the PN junction," Am. J. Phys. **62**, 66–70 (1994).
[4]L. Kirkup and F. Placido, "Undergraduate experiment: Determination of the band gap in germanium and silicon," Am. J. Phys. **54**, 918–920 (1986).
[5]B. D. Sukheeja, "Measurement of the band gap in silicon and germanium," Am. J. Phys. **51**, 72 (1983).
[6]P. J. Collings "Simple measurement of the band gap in silicon and germanium," Am. J. Phys. **48**, 197–199 (1980).
[7]N. J. Pinto, "Two experiments in physics based on electrospun polymer nanofibers," Am. J. Phys. **76**, 1163–1167 (2008).
[8]J. Brody, Z. Dong, and T. Dennen, "Inexpensive fabrication of silicon Hall devices," Am. J. Phys. **74**, 240–242 (2006).
[9]D. W. Preston and E. R. Dietz, *The Art of Experimental Physics* (Academic Press, San Diego, 2003), Chap. 17, pp. 303–315.
[10]A. C. Melissinos and J. Napolitano, *Experiments in Modern Physics*, 2nd ed. (Academic Press, San Diego, 2003), Chap. 3, Section 3, pp. 441–442.
[11]R. H. Chow, "Study on diffusion and recombination of minority carriers by the method of photoconductive decay," Am. J. Phys. **52**, 842–844 (1984).
[12]A. Sconza, G. Galet, and G. Torzo, "An improved version of the Haynes-Shockley experiment with electrical or optical injection of the excess carriers," Am. J. Phys. **68**, 80–87 (2000).
[13]M. D. Sturge and Song Bac Toh, "An experiment to demonstrate the canonical distribution," Am. J. Phys. **67**, 1129–1131 (1999).
[14]J. M. Essick and R. T. Mather, "Characterization of a bulk semiconductors band gap via a near-absorption edge optical transmission experiment," Am. J. Phys. **61**, 646–649 (1993).
[15]E. Redondo, A. Ojeda, G. Gonzalez Daz, and I. Martil, "A laboratory experiment with blue light-emitting diodes," Am. J. Phys. **65**, 371–376 (1997).
[16]I. Martil and G. Gonzalez Daz, "Undergraduate laboratory experiment: Measurement of the complex refractive index and the band gap of a thin film semiconductor," Am. J. Phys. **60**, 83–86 (1992).
[17]T. A. Laubach, L. A. Elizondo, P. J. McCann, and S. Gilani, "Quantum dotting the "i" of Inquiry: A guided inquiry approach to teaching nanotechnology," Phys. Teach. **48**, 186–188 (2010).
[18]J. Brody, D. Weiss, and P. Young, "Observing the Maxwell-Boltzmann distribution in LED emission spectra," Am. J. Phys. **78**, 933–935 (2010).
[19]A. Singha P. Dhar, and A. Roy "A nondestructive tool for nanomaterials: Raman and photoluminescence spectroscopy," Am. J. Phys. **73**, 224–233 (2005).
[20]D. K. Schroder, *Semiconductor Material and Device Characterization*, 3rd ed. (John Wiley and Sons, New Jersey, 2006), Chaps. 2 and 3.
[21]D. K. Schroder, *Semiconductor Material and Device Characterization*, 3rd ed. (John Wiley and Sons, New Jersey, 2006), p. 94.
[22]B. Streetman and S. Banerjee, *Solid State Electronic Devices*, 5th ed. (Prentice-Hall, New Jersey, 2000), pp. 202–205.
[23]S. M. Sze and K. K. Ng, *Physics of Semiconductor Devices*, 3rd ed. (Wiley-Interscience, New Jersey, 2006), Chaps. 2 and 3.
[24]S. M. Sze and K. K. Ng, *Physics of Semiconductor Devices*, 3rd ed. (Wiley-Interscience, New Jersey, 2006) p. 179–180

[25]F. R. Goodman, D. L. Heald, and R. C. Neville, "Laboratory experiment in semiconductor surface-field effects," Am. J. Phys. **42**, 572–579 (1974).
[26]P. Horowitz and W. Hill, *The Art of Electronics*, 2nd ed. (Cambridge U.P., New York, 1989), p. 1031.
[27]D. W. Preston and E. R. Dietz, *The Art of Experimental Physics* (Academic Press, San Diego, 2003) Chaps. 17, p. 367.
[28]Available from Mouser P/N 511-STPS20120D.
[29]While wearing proper protective lab wear (including gloves, safety glass, face shield) and working under a fume hood, the epoxy encapsulation of an electronic component such as a Schottky diode can be dissolved by applying drops of fuming nitric acid to the component while at elevated temperature (100 °C). After the electronic component is exposed, the part should be rinsed in methanol.
[30]Good results were also obtained on a smaller area Schottky diode (Vishay 844-11DQ10) with cylindrical encapsulation. We found that the encapsulation on this diode can be carefully cracked open using a vise and that, to a good approximation, the Schottky contact area is equal to the cross-sectional area of the diode's lead wire (0.49 mm^2).
[31]Performed by Evans Analytical Group, Sunnyvale, CA.
[32]W. Yang, "Teaching phase-sensitive demodulation for signal conditioning to undergraduate students," Am. J. Phys. **78**, 909–915 (2010).
[33]K. G. Libbrecht, E. D. Black, and C. M. Hirata, "A basic lock-in amplifier experiment for the undergraduate laboratory," Am. J. Phys. **71**, 1208–1213 (2003).
[34]J. H. Scofield, "Frequency domain description of a lock-in amplifier," Am. J. Phys. **62**, 129–133 (1994).
[35]R. Wolfson, "The lock-in amplifier: A student experiment," Am. J. Phys. **59**, 569–572 (1991).
[36]For the calibration capacitor, a 1-nF ceramic capacitor was used. Its actual capacitance value was determined to ±1% using an Agilent U1732B Handheld LCR Meter.
[37]S. E. Babcock and K. N. Tu, "Titanium-tungsten contacts to Si: The effects of alloying on Schottky contact and on silicide formation," J. Appl. Phys. **53**, 6898–6905 (1982).
[38]P. Blood, "Capacitance-voltage profiling and the characterisation of III-V semiconductors using electrolyte barriers," Semicond. Sci. Technol. **1**, 7–27 (1986).
[39]J. Essick, *Hands-On Introduction to LabVIEW for Scientists and Engineers*, 2nd ed. (Oxford U.P., New York, 2012) Chap. 10.
[40]R. Wolfson and D. Mullen, "Spreadsheet lock-in amplifier," Am. J. Phys. **78**, 1227–1229 (2010).
[41]Y. Kraftmakher, "Lock-in detection with DataStudio," Am. J. Phys. **74**, 207–210 (2006).
[42]P. J. Moriarty, B. L. Gallagher, C. J. Mellor, and R. R. Baines, "Graphical computing in the undergraduate laboratory: Teaching and interfacing with LabVIEW," Am. J. Phys. **71**, 1062–1704 (2003).
[43]See supplementary material at http://dx.doi.org/10.1119/1.4864162 for the LabVIEW programs.
[44]Both DAQ devices are available from National Instruments, Austin, TX.

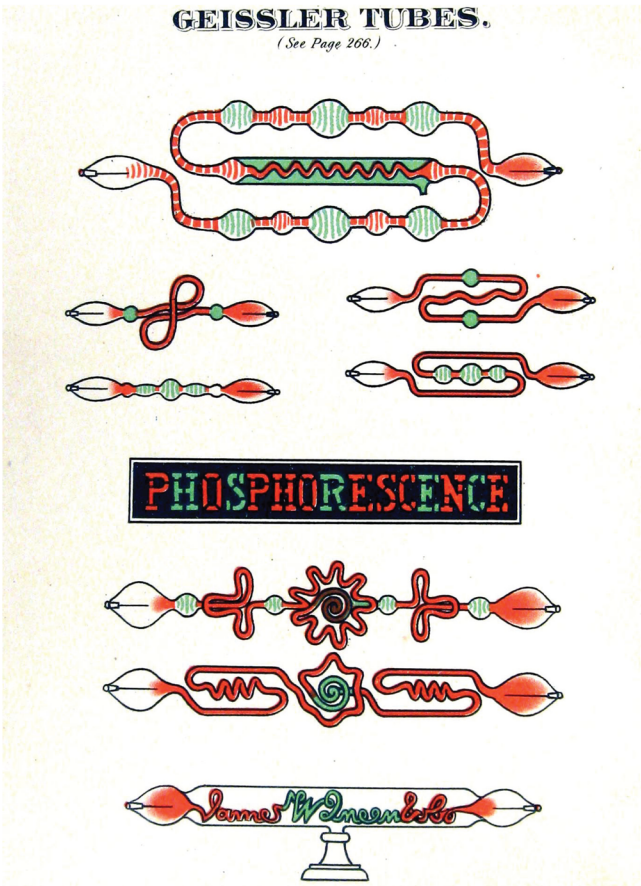

Geissler Tubes

"Geissler tubes are sealed glass tubes containing highly-rarified gases or vapors. The tube is filled with the gas or vapor, which is nearly all removed with a Sprengel air-pump. Platinum wires are sealed in the ends to make the connection through the glass. Electrical discharges through Geissler tubes produce brilliant and beautiful effects. The color of the light varies with the gas, air and nitrogen emitting a red color, carbonic acid [carbon dioxide] green, etc. Fluorescent substances, as uranium glass and sulphate of quinine, are often introduced to increase the brilliancy of the effect." From Thomas D. Baker, *Elements of Natural Philosophy, based on the Experimental Method* (The Werner Company, Chicago, 1881), frontispiece and pg 266. (Text by Thomas B. Greenslade, Jr., Kenyon College)